Coherent x-ray scattering from ultrathin probe layers

R. Röhlsberger
Technische Universität München, Physikdepartment E13, James-Franck-Str. 1, 85747 Garching, Germany

T. Klein and K. Schlage
Universität Rostock, Fachbereich Physik, August-Bebel-Str. 55, 18051 Rostock, Germany

O. Leupold and R. Rüffer
European Synchrotron Radiation Facility, Boîte Postale 220, 38043 Grenoble Cedex, France
(Received 20 October 2003; published 25 June 2004)

We have studied x-ray grazing incidence reflection from ultrathin layers that are embedded in thin film systems. This technique can be applied to selectively probe the properties of stratified media as a function of depth. A remarkable coherent enhancement of the reflected intensity renders this technique sensitive to ultrathin layers in the monolayer range. We investigate this enhancement theoretically and show that the coherently scattered signal is proportional to the square of the normalized field intensity at the position of the probe layer. This is in contrast to incoherent scattering from such probe layers where the signal scales linearly with the normalized field intensity at the position of the probe layer. The coherent enhancement is investigated experimentally by nuclear resonant scattering of synchrotron radiation from ultrathin isotopic layers of ^{57}Fe. The technique can be applied to all fields of coherent x-ray scattering from thin films.

DOI: 10.1103/PhysRevB.69.235412 PACS number(s): 61.10.Kw, 76.80.+y, 78.70.Ck, 07.85.Qe

I. INTRODUCTION

X-ray standing waves have a longstanding history in the field of x-ray analysis. This method has become an established tool for the analysis of adsorbates and ultrathin films on surfaces of single crystals.[1,2] The standing wave has the same periodicity as the diffracting lattice planes, and the phase of the wave field can be tuned by variation of the incidence angle within the Darwin width of the reflection. By monitoring the atomic fluorescence yield from the adsorbed species, their position relative to the diffracting lattice planes can be determined. This method can be applied also in the lowest-order Bragg-reflection, i.e., the (000) reflection which corresponds to grazing-incidence geometry. In this geometry, the period of the standing wave is given by $2\pi/q_z$ where q_z is the momentum transfer along the surface normal. Therefore, x-ray standing waves can be used for the investigation of thin films with a thickness of several nanometers. If the film thickness matches an integer multiple of the period of the standing-wave field, the intensity of the electric field inside the layer is resonantly enhanced. Then the partial waves that are multiply reflected at the boundaries of the film, add up constructively. The standing wave that forms as a result of such multibeam interference between the incident and the reflected wave can be used as the primary wave for structural analysis of the guiding layer. First experiments of this kind were reported by Wang *et al.*[3] who used the standing waves that formed in a macromolecular film on a metal substrate to obtain structural information about the film. The strong enhancement of the field intensity in the guiding layer was used to probe the vibrational properties of thin films via inelastic nuclear resonant scattering.[4,5] The intensity in the antinodes of the wave field can be even more enhanced by sandwiching the guiding layer between two layers of higher electron density, thus forming an x-ray waveguide structure.[6] This approach was systematically investigated by Sinha and coworkers.[7,8] Moreover, it was shown that the strong enhancement of the fluorescence yield from ultrathin probe layers can be used for structural characterization of metallic multilayers.[9,10] In all of these studies the measured signal was the fluorescence from individual atoms which is an *incoherent* scattering process. In this case the signal scales linearly with the integrated x-ray intensity within the layer under study.

Recently, standing waves in thin films were used for the analysis of liquid films,[11–13] biomolecular layers,[14,15] and the production of x-ray nanobeams.[16,17] In all these cases the signal resulted from a *coherent* scattering process like surface diffraction [14] or grazing incidence reflection. Due to the formation of standing waves in the film, the intensity of the radiation that is coherently scattered from any kind of matter within the wave field can be strongly amplified. In this paper we show that this coherent enhancement is qualitatively different from the intensity enhancement in the incoherent scattering channels. In particular, one finds an intensity amplification in the coherent scattering channels that is much stronger than the relative enhancement in the incoherent scattering channels. This can be exploited to investigate the properties of thin film systems by placing probe layers in selected depths of the system. The coherent enhancement of the scattered signal renders this technique very sensitive to smallest amounts of material like ultrathin films in the monolayer regime. Here we focus on coherent x-ray scattering from such ultrathin probe layers that are located in standing wave fields.

This paper is organized as follows: To establish a relation between the field intensity inside a layer structure and the specularly reflected signal, we first introduce a matrix formalism to calculate the amplitude of the electric field as function of depth. This will be illustrated for the particular

 ©2004 The American Physical Society

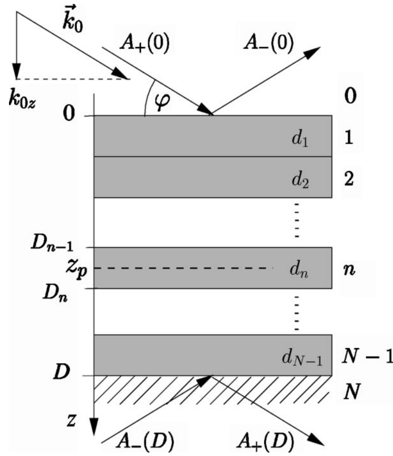

FIG. 1. Scheme of the layer system used here to describe x-ray propagation in stratified media. The incident wave is divided into two scattering channels, corresponding to specular reflection (–) and forward transmission (+). The layers labeled by 0 and N denote vacuum and substrate, respectively. The layer system contains an ultrathin probe layer (dashed line) in depth z_p within the nth layer.

case of x-ray waveguide structures where a strong enhancement of the normalized intensity inside the guiding layer is observed. In the following section, this matrix formalism is applied to express the reflectivity of an arbitrary layer system in terms of the scattering amplitude of an ultrathin layer that is embedded anyhere in the system. The remarkable result is that the reflected intensity from the probe layer is proportional to the square of the normalized field intensity at its position in the layer system. In the next section this relation is verified experimentally via nuclear resonant scattering from isotopic probe layers of ^{57}Fe. A number of possible applications for coherent x-ray scattering from ultrathin probe layers will be discussed.

II. X RAYS IN STRATIFIED MEDIA

In this section we calculate the x-ray intensity inside arbitrary layer systems. While there are a number of matrix-based formalisms that treat purely electronic (isotropic) scattering,[18,19] the formalism presented here takes into account the full polarization dependence of the (anisotropic) scattering process. This allows one to treat scattering processes that exhibit strong polarization mixing effects and optical activity like magnetic x-ray scattering or nuclear resonant scattering. The formalism used here is a matrix version of the dynamical theory of coherent x-ray scattering. The matrix elements can be considered as transition amplitudes between the open scattering channels, including the polarization states of the radiation. This formalism was extended to the description of grazing incidence reflection from thin films.[20,21] In this geometry, two scattering channels are open, i.e., forward transmission (+) and specular reflection (–). The nomenclature of the layer system and the scattering geometry is introduced in Fig. 1. For a theoretical description, the fields in the open scattering channels are combined into one supervector $\boldsymbol{A}=(A_+,A_-)$. In a single layer, labeled by index n, the field amplitude $\boldsymbol{A}(z)$ in depth z is then related to the field amplitude $\boldsymbol{A}(0)$ at the surface by[20,21]

$$\boldsymbol{A}(z)=e^{i\mathbf{F}_n z}\boldsymbol{A}(0)=:\mathbf{L}_n(z)\boldsymbol{A}(0), \tag{1}$$

with $\mathbf{F}_n$ being the so-called propagation matrix that is given by

$$\mathbf{F}_n=\begin{pmatrix} \mathbf{f}_n+\mathbf{k}_{0z} & \mathbf{f}_n \\ -\mathbf{f}_n & -\mathbf{f}_n-\mathbf{k}_{0z} \end{pmatrix}, \tag{2}$$

where

$$\mathbf{f}_n=\frac{2\pi}{k_{0z}}\sum_j \rho_j \mathbf{M}_j(\omega) \tag{3}$$

is the scattering matrix for grazing incidence reflection. The matrix $\mathbf{L}_n(z)$ that was introduced in Eq. (1) is called the layer matrix of layer n. The sum in Eq. (3) runs over all atomic species in the layer with number densities ρ_j each and the energy-dependent forward scattering length $\mathbf{M}_j(\omega)$ which is a 2×2 matrix to account for the polarization dependence of the scattering process, as explained in the following section. $\mathbf{k}_{0z}=k_{0z}\,\mathbf{1}$, where $k_{0z}\approx k_0\varphi$ is the z component of the wave vector and $\mathbf{1}$ is the 2×2 unit matrix.

In the general case of multiple layers ($N-1$ layers with thicknesses d_n on a substrate), the field amplitudes in depth z of the sample is simply given by the matrix product of the corresponding layer matrices

$$A(z)=\mathbf{L}(z)A(0), \tag{4}$$

with

$$\mathbf{L}(z)=\mathbf{L}_n(z-D_{n-1})\ldots\mathbf{L}_2(d_2)\mathbf{L}_1(d_1). \tag{5}$$

This formalism can be applied to a variety of phenomena like Bragg and Laue diffraction from single crystals, diffraction from planar gratings and grazing-incidence reflection from thin-film systems. It allows, in a natural way, to accomodate the polarization dependence of the scattering as it arises in magnetic x-ray scattering or nuclear resonant scattering. The mathematical problem in any of these cases is the calculation of the exponential of the propagation matrix $\mathbf{F}$. Since there is no analytic solution in general, this problem has to be solved numerically in most cases. However, in special situations a closed solution can be found that reduces the computational effort and provides physical insight. This applies for scattering in grazing incidence geometry which shall be considered in the following.

The formalism is considerably simplified in the system of eigenpolarizations of the system. Those are obtained by diagonalization of $\mathbf{f}$:

$$\mathbf{f}_{n,D}=\mathbf{g}\mathbf{f}_n\mathbf{g}^{-1}, \tag{6}$$

with the diagonalizing matrix $\mathbf{g}$, the eigenvalues $f_{n,\mu}(\omega)$ of the matrix $\mathbf{f}_n$, and $[\mathbf{f}_{n,D}]_{\mu\nu}=\delta_{\mu\nu}f_{n,\mu}$. In this case the problem can be solved for each eigenpolarization separately. Thus, for better readability, we drop the polarization index μ in the following paragraph.

Due to the symmetry of the propagation matrix $\mathbf{F}$, the layer matrix of a freestanding single layer can now be written in a very compact form

$$\mathbf{L}_1(z)=e^{i\mathbf{F}_1 z}=\frac{1}{t_{01}}\begin{pmatrix}1 & r_{01}\\ r_{01} & 1\end{pmatrix}\begin{pmatrix}e^{ik_{1z}z} & 0\\ 0 & e^{-ik_{1z}z}\end{pmatrix}\begin{pmatrix}1 & r_{10}\\ r_{10} & 1\end{pmatrix}\frac{1}{t_{10}}. \tag{7}$$

k_{1z} is the z component of the wave vector in the film, which is through Snell's law related to the z component of the incident wave vector by

$$k_{1z}=k_{0z}\beta_1 \text{ with } \beta_1=\sqrt{1+\frac{2f_1}{k_{0z}}}. \tag{8}$$

$r_{ij}=(\beta_i-\beta_j)/(\beta_i+\beta_j)$ and $t_{ij}=2\beta_i/(\beta_i+\beta_j)$ are the Fresnel reflection and transmission coefficients of the boundary between the media i and j, respectively. Equation (7) represents a very intuitive description of the scattering process that can be read from right to left: The right matrix describes the transition of the wavefield at the boundary from the vacuum (0) into the medium (1), the middle matrix describes the free propagation of the eigenpolarizations in the medium in (+) and (−) directions, and the left matrix describes the transition of the wave field back into vacuum.

The matrix product for the whole layer system shown in Fig. 1 is then given by

$$\mathbf{L}(D)=\mathbf{L}_N\mathbf{L}_{N-1}(d_{N-1})\ldots\mathbf{L}_2(d_2)\mathbf{L}_1(d_1). \tag{9}$$

Due to its very large thickness, the layer matrix $\mathbf{L}_N$ of the substrate requires a special treatment, resulting in

$$\mathbf{L}_N=\begin{pmatrix}0 & 0\\ 0 & 1\end{pmatrix}\begin{pmatrix}1 & r_{N0}\\ r_{N0} & 1\end{pmatrix}\frac{1}{t_{N0}}. \tag{10}$$

The left matrix reflects the fact that the wave propagating into the substrate vanishes with increasing depth so that only waves in the specular direction remain.

To solve for the specularly reflected and forward transmitted fields, we decompose Eq. (4) into its components in the two scattering channels

$$\begin{pmatrix}A_+(z)\\ A_-(z)\end{pmatrix}=\begin{pmatrix}L_{++} & L_{+-}\\ L_{-+} & L_{--}\end{pmatrix}\begin{pmatrix}A_+(0)\\ A_-(0)\end{pmatrix}. \tag{11}$$

For a unique solution of the fields in the scattering channels, the boundary conditions have to be supplied

$$A_+(0)=A_0,\quad A_-(D)=0. \tag{12}$$

Now one can solve this equation for the specularly reflected field $A_-(0)$ and the forward transmitted field $A_+(D)$:

$$A_-(0)=-\left[\frac{L_{-+}(D)}{L_{--}(D)}\right]A_0=:RA_0, \tag{13}$$

$$A_+(D)=\left[L_{++}(D)-\frac{L_{+-}(D)L_{-+}(D)}{L_{--}(D)}\right]A_0. \tag{14}$$

With this solution, Eq. (11) can now be used to calculate the amplitude $A(z)$ of the electric field in depth z of the layer system. This amplitude is given by the superposition of the waves in depth z traveling in (+) and (−) directions, i.e.:

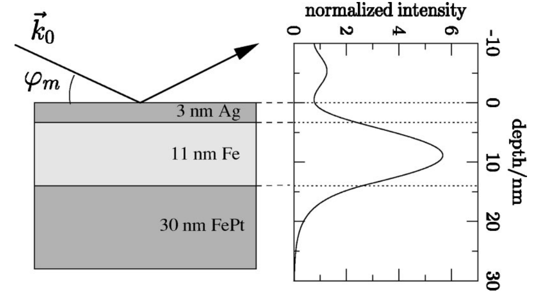

FIG. 2. Grazing incidence x-ray reflection from a waveguide structure consisting of two exchange-coupled magnetic layers (Fe/FePt) covered with Ag (left). This forms an x-ray waveguide, resulting in a sixfold enhancement of the intensity in the center of the Fe guiding layer (right).

$$A(z)=A_+(z)+A_-(z). \tag{15}$$

Inserting Eq. (13) into Eq. (11), we obtain for the normalized field amplitude $a(z)$ in depth z of the layer system

$$a(z)=\frac{A(z)}{A_0}=L_{++}(z)+L_{-+}(z)-[L_{+-}(z)+L_{--}(z)]\frac{L_{-+}(D)}{L_{--}(D)}. \tag{16}$$

Using this formula, the field intensity in arbitrary layer systems can be calculated. An example is shown in Fig. 2 for a trilayer system consisting of Ag/Fe/FePt on Si that was investigated in this study. Due to the electron density profile of this layer stack, the radiation that is evanescently coupled into the Fe layer will be multiply reflected at the layer boundaries. Since the energy transport takes place parallel to the boundaries, such layer systems can be regarded as x-ray waveguides.[7] Depending on the film thickness, a certain number of guided modes can be excited, which show up as minima in the reflectivity of the layer system between the critical angles of the layer and the substrate material. The layer system shown here is a single-mode waveguide where the guided TE_0 mode is excited at an angle of incidence of $\varphi=4.3$ mrad. In the center of the guiding layer a six-fold enhancement of the x-ray intensity is observed. That effect was employed to image the magnetic structure of such layer systems via nuclear resonant x-ray scattering.[22] In this experiment, an ultrathin probe layer of ^{57}Fe was embedded in various depths of the Fe layer. Due to its placement in the standing wave field of the x-ray waveguide, the resonant signal from this probe layer was strongly enhanced. This will be investigated quantitatively in the following.

III. COHERENT REFLECTION FROM ULTRATHIN PROBE LAYERS

In this section we calculate the reflectivity from an ultrathin probe layer that is embedded in an arbitrary layer system. Such an ultrathin film can be used as a probe layer to investigate the internal magnetic, electronic, or structural properties of stratified media with very high spatial resolution. We assume this probe layer of thickness d being located in depth z_p of the layer system within the nth layer of the

system, as sketched in Fig. 1. To calculate the reflectivity of this system, we write the field amplitude in depth D of the layer system as follows:

$$A(D)=\mathbf{L}(D-z_p)\mathbf{L}_n(d)\mathbf{L}(z_p)A_0. \tag{17}$$

This equation expresses the fact that the probe layer is sandwiched between two layer stacks of total thickness z_p and $D-z_p$. It follows from the definition in Eq. (5) that

$$\mathbf{L}(D-z_p)=\mathbf{L}(D)\mathbf{L}^{-1}(z_p). \tag{18}$$

Then Eq. (17) can be written as

$$A(D)=\mathbf{L}(D)\mathbf{L}^{-1}(z_p)\mathbf{L}_n(d)\mathbf{L}(z_p)A_0. \tag{19}$$

For an ultrathin layer, the matrix $\mathbf{L}_n(d)=e^{i\mathbf{F}_n d}$ can be approximated by

$$\mathbf{L}_n(d)\approx 1+i\mathbf{F}_n d, \tag{20}$$

with the propagation matrix being the following 2×2 matrix

$$\mathbf{F}_n=\begin{pmatrix} f_n+k_{0z} & f_n \\ -f_n & -f_n-k_{0z}\end{pmatrix}, \tag{21}$$

where f_n is the scattering amplitude of the probe layer material for one of the eigenpolarizations. Equation (19) then turns into

$$\begin{aligned} \boldsymbol{A}(D)&=[\mathbf{L}(D)\mathbf{L}^{-1}(z_p)(1+i\mathbf{F}_n d)\mathbf{L}(z_p)]\boldsymbol{A}_0 \\ &=\mathbf{L}(D)[1+id\mathbf{L}^{-1}(z_p)\mathbf{F}_n\mathbf{L}(z_p)]\boldsymbol{A}_0, \end{aligned} \tag{22}$$

with $\mathbf{L}(z_p)$ as defined in Eq. (11) and $\mathbf{L}(D)$ written as

$$\mathbf{L}(D)=\begin{pmatrix} D_{++} & D_{+-} \\ D_{-+} & D_{--}\end{pmatrix}. \tag{23}$$

The inverse of the matrix $\mathbf{L}(z_p)$ is given by

$$\mathbf{L}^{-1}(z_p)=\begin{pmatrix} L_{--} & -L_{+-} \\ -L_{-+} & L_{++}\end{pmatrix}, \tag{24}$$

where we have already used the fact that $\det(\mathbf{L}_n)=1$, as can be easily verified via Eq. (7). This implies that also the determinant of $\mathbf{L}(z)$, i.e., any product of matrices $\mathbf{L}_n$ equals 1. Performing the matrix multiplications in Eq. (22), the reflectivity according to Eq. (13) is given by

$$R=-\frac{D_{-+}(1+idE_{++})+idD_{--}E_{-+}}{D_{--}(1+idE_{--})+idD_{-+}E_{+-}}, \tag{25}$$

with

$$\begin{aligned} E_{++}&=-E_{--} \\ &=(L_{++}+L_{-+})(L_{--}+L_{+-})f_n+(L_{++}L_{--}+L_{+-}L_{-+})k_{0z} \end{aligned} \tag{26}$$

$$E_{+-}=(L_{--}+L_{+-})^2 f+2L_{--}L_{+-}k_{0z} \tag{27}$$

$$E_{-+}=-(L_{++}+L_{-+})^2 f-2L_{++}L_{-+}k_{0z}. \tag{28}$$

Expanding Eq. (25) up to first order in (id) leads to

$$R\approx R_0+id(2R_0E_{++}+E_{-+}-R_0^2E_{+-}), \tag{29}$$

with $R_0=-(D_{-+}/D_{--})$ being the reflectivity of the layer system without the probe layer. Inserting Eqs. (26)–(28) into Eq. (29), one obtains

$$\begin{aligned} R=R_0&+id\, f_n[(L_{++}+L_{-+})+(L_{+-}+L_{--})R_0]^2 \\ &-2id\, k_{0z}(R_0L_{--}+L_{-+})(R_0L_{+-}+L_{++}). \end{aligned} \tag{30}$$

By comparison with Eq. (11) and taking into account that $A_-(0)=RA_0$, this equation can be written as

$$\begin{aligned} R(\omega)=R_0&+id\, f_n(\omega)[A_+(z_p)+A_-(z_p)]^2/A_0^2 \\ &+2id\, k_{0z}\, A_+(z_p)A_-(z_p)/A_0^2. \end{aligned} \tag{31}$$

To indicate the energy dependence of this equation, it is written as function of frequency ω. The expression in the square brackets is exactly the normalized field amplitude $a(z_p)$ at the position z_p of the probe layer, as given by Eq. (16). The last term in Eq. (31) is a geometric contribution that does not depend on energy. Thus, the energy dependent contribution $R_n(\omega)$ of the probe layer to the reflectivity is given by the term that is proportional to $f_n(\omega)$. Performing the transformation back into the original polarization basis, we obtain

$$\mathbf{R}_n(\omega)=id\, a(z_p)^2\mathbf{f}_n(\omega), \tag{32}$$

where $\mathbf{R}_n$ and $\mathbf{f}_n$ appear as 2×2 matrices. As has been shown here, this relation results from a perturbation expansion that is valid as long as the modulus of the second-order term in Eq. (20) is smaller than, say, 0.1. This leads to the condition $(k_{0z}d)^2<0.1$, from which one derives $d<1.0$ nm at a photon energy of 14.4 keV and an angle of incidence of 4 mrad. In any case, however, the layer thickness should be sufficiently small to keep the averaging over the depth dependent properties to a minimum. In this sense the earlier limit may be too coarse in special cases, in particular when the total thickness of the layer under study is not significantly larger than the probe layer thickness.

Equation (32) is the central result of this paper. A similar relation was suggested recently by Andreeva *et al.*, for the special case of an ultrathin film on the surface of a layer system.[23] Here we have derived rigorously the contribution of an ultrathin film to the total reflectivity of the layer system where it is embedded in. For an experimental verification of this relation, we have performed nuclear resonant scattering from ultrathin isotopic layers consisting of ^{57}Fe, as described in the following section.

IV. NUCLEAR RESONANT X-RAY SCATTERING

Up to here the formalism was quite general and can be applied to any case of coherent x-ray scattering process. Due to its pronounced energy dependence, nuclear resonant scattering is an ideal technique to verify the dependence of the reflected amplitude $\mathbf{R}_n(\omega)$ on the field amplitude $a(z_p)$ as described by Eq. (32).

Coherent nuclear resonant scattering from thin films and multilayers became a routine technique after the advent of high-brilliance synchrotron radiation sources.[24–28] A particu-

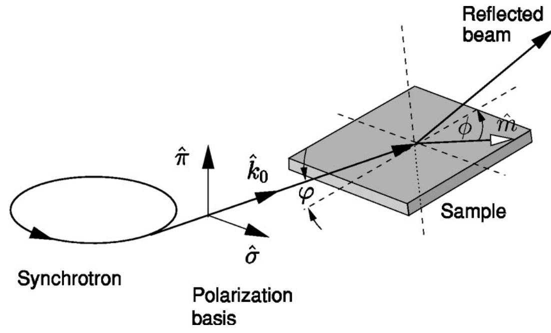

FIG. 3. Scattering geometry used in the experiments described here. The sketch shows the relative orientation of the incident wave vector $\hat{k}_0$ to the direction of a unidirectional magnetization $\hat{m}$ in the plane of the sample. $(\hat{\sigma},\hat{\pi})$ are the linear polarization basis vectors.

lar application in this field is the use of ultrathin isotopic probe layers with a thickness of a few angstroms to study depth dependent properties in layered systems. This method has been applied in conventional Mössbauer spectroscopy for a long time. [29–33] It is the virtue of this technique that isotopic probe layers do not disturb the chemical integrity of the system under study. Compared to the conventional technique, data acquisition times at modern synchrotron radiation sources are reduced by orders of magnitude, triggering new applications in this field.[22,34,35]

The time response from ultrathin isotopic probe layers is obtained by Fourier transformation of Eq. (32):

$$\tilde{\mathbf{R}}_n(t) = id\ a(z_p)^2\,\tilde{\mathbf{f}}_n(t). \tag{33}$$

The 14.4 keV resonance of ^{57}Fe is a magnetic dipole transition with spins $I_g=1/2$ and $I_e=3/2$ of the ground and excited state, respectively, and a natural lifetime of $\tau_0=141$ ns. A purely magnetic hyperfine interaction lifts the degeneracy of the magnetic sublevels, resulting in six dipole-allowed transitions where the level splittings of the ground and excited state are given by Δ_g and Δ_e, respectively. For calculation of the scattered intensity, $I(t)$, we take into account the scattering geometry shown in Fig. 3, assuming the standard experimental situation with incident σ polarization and no polarization analysis in the detection process. This leads to

$$I(t) = d^2 I_p^2 I_n(t), \tag{34}$$

where $I_p=|a(z_p)|^2$ is the normalized intensity of the electric field at the position of the probe layer. If we assume that the magnetization is confined to the plane of the sample, the delayed intensity $I_n(t)$ can be written as [21]

$$I_n(t) = e^{-\chi t/\tau_0}[G(0,0,\Omega_1)(1+\cos^2\phi) + G(\Omega_1+\Omega_2,\Omega_1-\Omega_2,\Omega_2)(1-\cos^2\phi)], \tag{35}$$

where the function G is given by

$$G(c_1,c_2,c_3) = \cos c_1 t + \tfrac{1}{9}\cos c_2 t + \tfrac{2}{3}\cos c_3 t, \tag{36}$$

and $\hbar\Omega_1=\Delta_e+\Delta_g$, $\hbar\Omega_2=2\Delta_e$. The angle ϕ is the azimuthal angle of the in-plane magnetization, as defined in Fig. 3. χ is a parameter that describes the speedup of the nuclear decay due to multiple scattering events.[36] For small values, $\chi<2$, this effect can be described simply by an additional exponential that can be factored out. For significantly larger values, the time response is significantly perturbed by an additional beat phenomenon, the so-called dynamical beat.[37]

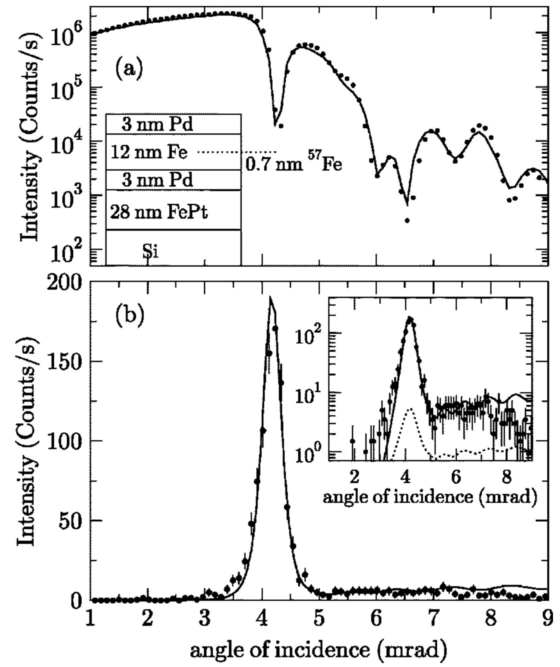

FIG. 4. (a) Measured electronic reflectivity from the layer system shown in the inset (*sample 1*). In the center of the guiding layer (Fe), an ultrathin film of 0.7 nm ^{57}Fe is embedded. At the minimum at φ_m = 4.3 mrad, the radiation couples into the first-order guided mode. The solid line is the calculated reflectivity of the layer system sketched here with an average interface roughness of 0.5 nm. (b) Time-integrated delayed intensity from the layer system, recorded within a time window from 20 to 160 ns after excitation. The inset shows the same data on a logarithmic scale. The dashed line is the normalized intensity of the electric field at the position of the ^{57}Fe layer. The solid lines are the square of this curve, scaled to the measured data.

V. EXPERIMENTS

The samples used in this experiment were the following layer systems: (3 nm Pd)/(11 nm Fe)/(3 nm Pd)/(28 nm FePt in the $L1_0$ phase), further denoted as *sample 1*, and (3 nm Ag)/(11 nm Fe)/(28 nm FePt in the $L1_0$ phase), further denoted as *sample 2*. In the Fe layers in both samples, a 0.7-nm-thick probe layer of ^{57}Fe was embedded, as sketched in Figs. 4(a) and 6. Both layer systems were produced by radio frequency magnetron sputtering in Ar atmosphere at a pressure of 1.0×10^{-2} mbar on superpolished Si wafers with a roughness below 0.5 nm root-mean-square. Details about the sample preparation are given in Ref. 22. The preparation of these layer systems was motivated by the investigation of the in-depth spin structure in a soft-magnetic layer (Fe) that is exchange-coupled to a hard-magnetic layer (FePt). Such systems are well known as so-called exchange-spring magnets.[38,39] They are interesting candidates for the development of new materials for permanent magnets [40] and

serve as model systems for the study of spin-dependent electronic transport properties.[41] In external magnetic fields, a spiral magnetic spin structure in the soft-magnetic layer develops.[39] This spin structure has been studied via polarized neutron scattering and the application of a specially developed reconstruction algorithm.[42] Recently, this spin structure was measured directly by nuclear resonant scattering of synchrotron radiation from ultrathin isotopic probe layers.[22] These measurements significantly benefitted from the intensity enhancement due to the formation of standing waves in the soft-magnetic layer. Due to their electron density profile, the earlier mentioned layer systems constitute x-ray waveguides with the guiding layer consisting of Fe, sandwiched between highly reflective Pd (Ag) and FePt layers.

The experiments were performed at the Nuclear Resonance beamline (ID18) of the ESRF [43] in the scattering geometry shown in Fig. 3. In the first experiment, we used *sample 1* to study the dependence of the coherent intensity enhancement as a function of the angle of incidence. At the sample position, the beam cross section was 150 μm (vertical) $\times$ 200 μm (horizontal). In this experiment, the sample was mounted in a cryomagnet system, cooled to 4 K and subjected to a transverse magnetic field of B=40 mT, as shown in Fig. 3. Figure 4(a) displays the angular dependence of the electronic (charge scattering) reflectivity. The first-order guided mode shows up at 4.3 mrad as a pronounced dip in the electronic reflectivity. The solid line is a fit according to Eq. (13), assuming the layer structure shown in the inset. Figure 4(b) shows the resonant signal from the ^{57}Fe probe layer as obtained by taking the time-ingrated delayed signal within a time window ranging from 12 to 160 ns after excitation. Its angular dependence shows a strong peak at the angular position where the waveguide mode is excited. One observes a 36-fold enhancement of the intensity relative to the value obtained at large angles of incidence. For a better illustration of the relative intensities, the same data are shown in the inset on a logarithmic scale. The dashed line displays the normalized intensity of the electric field at the position of the ^{57}Fe layer. In the antinode of this TE_0 mode the intensity exhibits a sixfold enhancement relative to the intensity of the incident beam. Correspondingly, the coherently scattered signal displays a 36-fold enhancement. The solid line in both graphs is obtained by squaring the values of the dashed curve and scaling them to the measured data. The very good agreement verifies the quadratic dependence on the normalized intensity at the probe layer position as established in Eq. (34). To demonstrate the applicability of this method for magnetic measurements, we have recorded a time spectrum with the sample aligned to the maximum of the delayed intensity. This is shown in Fig. 5. The average delayed count rate in this geometry was about 220 s^{-1}, so that time spectra with very good statistical quality could be obtained within less than 10 min. The solid line is a fit to the data according to Eq. (35) from which an azimuthal angle of ϕ=45(2)° was derived for the orientation of the probe-layer magnetization $\hat{m}$ relative to the incident wave vector $\hat{k}_0$.[44] In contrast, data acquisition times in conventional Mössbauer spectroscopy with a radioactive source of 50 mCi activity that lead to a comparable statistical quality are in the range of 3–4 days.

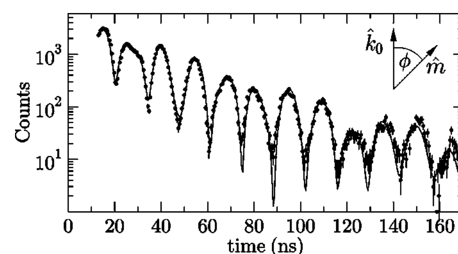

FIG. 5. Time spectrum of the Pd/Fe/Pd sample recorded at the angular position where the first-order guided mode is excited. Due to the intensity enhancement, a count rate of 220 s^{-1} was achieved in the time window displayed here, so that this spectrum could be recorded within 8 min. The solid line is a theoretical simulation from which an in-plane angle ϕ=45° of the magnetization relative to the incident wavevector was derived.

In another experiment the quadratic intensity dependence was verified in a different way. For this purpose, *sample 2* was mounted in the cryomagnet system, cooled to 4 K and subjected to an external field of 160 mT. The layer structure of this sample is illustrated in the top part of Fig. 6. The central element is a 0.7-nm-thick probe layer of ^{57}Fe that is embedded in the Fe layer with a slope between the two boundaries. Due to this slope, a linear relation between the transverse displacement of the sample relative to the beam and the depth of the probe layer is established. This was applied recently to measure the depth dependence of the magnetization rotation for such exchange-spring bilayers in external fields.[22] Figure 6 shows the time-integrated delayed intensity recorded as a function of depth of the probe layer.

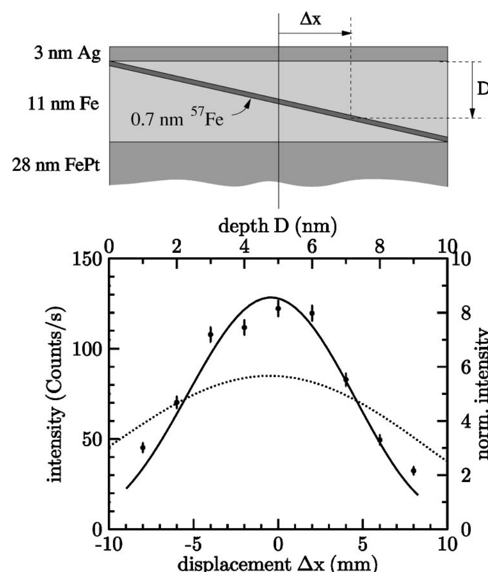

FIG. 6. Time-integrated signal as function of the transverse displacement Δx of *sample 2 relative* to the beam. Due to a tilted ^{57}Fe probe layer in the Fe layer, as sketched in the upper part, the transverse displacement maps the depth dependence of the reflected signal. The dashed line is the normalized field intensity as function of depth, the solid line is the square of this function, scaled to the measured data.

The sample was adjusted to the first-order waveguide mode at an angle of incidence of 4.4 mrad. The solid line is a fit to the data based on the square of the normalized field intensity at the probe layer position that is shown as dashed line. As can be seen already in Fig. 2, the field intensity in the guiding layer varies by a factor of 2 from the layer boundaries to the center of the layer. Due to the quadratic dependence on the field intensity, one expects the resonant signal to vary by a factor of 4. This is confirmed to a very good accuracy in this experiment.

VI. CONCLUSION

The experiments shown here have demonstrated the remarkable intensity enhancement that results from coherent x-ray scattering by ultrathin proble layers. This was verified experimentally by nuclear resonant scattering of synchrotron radiation from ultrathin isotopic probe layers of ^{57}Fe.

The central result of this paper, Eq. (32), can be compared with the description of nuclear resonant specular reflection in the distorted-wave Born approximation,[45] where the reflectivity of a surface is given by

$$R(\omega) = R_0 + T(k_i)T(k_f)R_n(\omega). \quad (37)$$

$T(k_i)$ and $T(k_f)$ are the Fresnel coefficients for transmission into the material (wave vector k_i) and transmission backout (wave vector k_f), respectively. These coefficients can be related to the reflection coefficients via $T=1+R$. This equation expresses the superposition of the incident amplitude a_0 and the reflected amplitude Ra_0, resulting in the field amplitude $a=(1+R)a_0$ at the boundary between the two media. Thus, in a more general approach, T should be replaced by the amplitude of the electric field at the layer boundary. In the special case of $k_i=k_f$ (specular reflection), the product $T(k_i)T(k_f)$ merges into $a(z)^2$ as in Eq. (32).

This quadratic dependence on the normalized intensity at the probe layer position leads to a very strong enhancement of the signal in the coherent scattering channels. In combination with x-ray waveguide structures this technique can be employed for signal amplification from smallest amounts of material. Thus, probe layers of monolayer thickness can be used to investigate the in-depth properties of thin films with unprecedented spatial resolution. It is obvious that this method can be applied to other Mössbauer isotopes as well. Moreover, this coherent enhancement effect is of course not restricted to nuclear resonant x-ray scattering. In can be exploited in many other areas where coherent reflection from stratified media is used. This is the case for magnetic x-ray scattering as well as polarized neutron scattering, for example.

While ultrathin layers can be used as probes to study selected parts of the sample, they may be the subject of investigation itself. An example could be a thin layer of clusters or nanoparticles that is embedded in the center of the guiding layer of an x-ray waveguide. If the photoabsorption in the guiding layer material is sufficiently low, as for elements like B, C, Al, coherent enhancement factors greater than 10^3 can be expected. This technique leads to a very strong signal enhancement in every kind of coherent x-ray scattering. Therefore, it also very attractive for off-specular methods that probe the in-plane structure of thin films and surfaces like grazing-incidence small-angle x-ray scattering. Moreover, it can be very beneficial also for spectroscopic methods that probe dynamical properties of condensed matter like inelastic x-ray spectroscopy and x-ray photon correlation spectroscopy. The enormous brilliance of modern synchrotron radiation sources allows for the application of focusing techniques to couple the incident radiation very efficiently into the waveguide modes. Extremely high signal-to-noise ratio can be expected, if this technique is used in combination with element-specific scattering techniques like coherent resonant x-ray scattering.

ACKNOWLEDGMENTS

This work was supported by the German BMBF under Contract No. 05 SK8HR 1. The authors kindly acknowledge the support of H. Thomas, S. Otto, K. W. Quast, and E. Burkel during the experiments.

[1] J. Zegenhagen, Surf. Sci. Rep. **18**, 199 (1993).

[2] D. E. Woodruff, Prog. Surf. Sci. **57**, 1 (1998).

[3] Y. Wang, M. Bedzyk, and M. Caffrey, Science **258**, 775 (1992).

[4] R. Röhlsberger, W. Sturhahn, T. S. Toellner, K. W. Quast, P. Hession, M. Hu, J. Sutter, and E. E. Alp, J. Appl. Phys. **86**, 584 (1999).

[5] R. Röhlsberger, W. Sturhahn, T. S. Toellner, K. W. Quast, E. E. Alp, A. Bernhard, J. Metge, R. Rüffer, and E. Burkel, Physica B **263–264**, 581 (1999).

[6] E. Spiller and A. Segmüller, Appl. Phys. Lett. **24**, 60 (1974).

[7] Y. P. Feng, S. K. Sinha, H. W. Deckman, J. B. Hastings, and D. P. Siddons, Phys. Rev. Lett. **71**, 537 (1993).

[8] Y. P. Feng, S. K. Sinha, E. E. Fullerton, G. Grübel, D. Abernathy, D. P. Siddons, and J. B. Hastings, Appl. Phys. Lett. **67**, 3647 (1995).

[9] S. K. Ghose and B. N. Dev, Phys. Rev. B **63**, 245409 (2001).

[10] S. K. Ghose, B. N. Dev, and A. Gupta, Phys. Rev. B **64**, 233403 (2001).

[11] M. J. Zwanenburg, J. F. Peters, J. H. H. Bongaerts, S. A. de Vries, D. L. Abernathy, and J. F. van der Veen, Phys. Rev. Lett. **82**, 1696 (1999).

[12] M. J. Zwanenburg, J. H. H. Bongaerts, J. F. Peters, D. O. Riese, and J. F. van der Veen, Phys. Rev. Lett. **85**, 5154 (2000).

[13] O. H. Seeck, H. Kim, D. R. Lee, D. Shu, I. D. Kaendler, J. K. Basu, and S. K. Sinha, Europhys. Lett. **60**, 376 (2002).

[14] F. Pfeiffer, T. Salditt, P. Hoghoj, and C. David, Proc. SPIE **4145**, 193 (2001).

[15] F. Pfeiffer, U. Mennicke, and T. Salditt, J. Appl. Crystallogr. **35**, 163 (2002).

[16] F. Pfeiffer, T. Salditt, P. Hoghoj, I. Anderson, and N. Schell, Phys.

Rev. B **62**, 16 939 (2000).
[17] F. Pfeiffer, C. David, M. Burghammer, C. Riekel, and T. Salditt, Science **297**, 230 (2002).
[18] B. Vidal and P. Vincent, Appl. Opt. **23**, 1794 (1984).
[19] A. Krol, C. J. Sher, and Y. H. Kao, Phys. Rev. B **38**, 8579 (1988).
[20] R. Röhlsberger, Hyperfine Interact. **123/124**, 301 (1999).
[21] R. Röhlsberger, J. Bansmann, V. Senz, K. L. Jonas, A. Bettac, K. H. Meiwes-Broer, and O. Leupold, Phys. Rev. B **67**, 245412 (2003).
[22] R. Röhlsberger, H. Thomas, K. Schlage, E. Burkel, O. Leupold, and R. Rüffer, Phys. Rev. Lett. **89**, 237201 (2002).
[23] M. A. Andreeva and B. Lindgren, Pis'ma Zh. Eksp. Teor. Fiz. **76**, 833 (2002).
[24] R. Röhlsberger, E. Gerdau, E. Lüken, H. D. Rüter, J. Metge, and O. Leupold, Z. Phys. B: Condens. Matter **92**, 489 (1993).
[25] A. I. Chumakov, G. V. Smirnov, A. Q. R. Baron, J. Arthur, D. E. Brown, S. L. Ruby, G. S. Brown, and N. N. Salashchenko, Phys. Rev. Lett. **71**, 2489 (1993).
[26] T. S. Toellner, W. Sturhahn, R. Röhlsberger, E. E. Alp, C. H. Sowers, and E. E. Fullerton, Phys. Rev. Lett. **74**, 3475 (1995).
[27] A. I. Chumakov, L. Niesen, D. L. Nagy, and E. E. Alp Hyperfine Interact. **123/124**, 427 (1999).
[28] D. L. Nagy, L. Bottyán, B. Croonenborghs, L. Deák, B. Degroote, J. Dekoster, H. J. Lauter, V. Lauter-Pasyuk, O. Leupold, M. Major, J. Meersschaut, O. Nikonov, A. Petrenko, R. Rüffer, H. Spiering, and E. Szilágyi, Phys. Rev. Lett. **88**, 157202 (2002).
[29] J. Tyson, A. H. Owens, J. C. Walker, and G. Bayreuther, J. Appl. Phys. **52**, 2487 (1981).
[30] J. Korecki and U. Gradmann, Phys. Rev. Lett. **55**, 2491 (1985).
[31] G. Lugert and G. Bayreuther, Phys. Rev. B **38**, 11068 (1988).
[32] M. Przybylski, I. Kaufmann, and U. Gradmann, Phys. Rev. B **40**, 8631 (1989).
[33] T. Shinjo, Surf. Sci. Rep. **12**, 49 (1991).
[34] L. Niesen, A. Mugarza, M. F. Rosu, R. Coehoorn, R. M. Jungblut, F. Roozeboom, A. Q. R. Baron, A. I. Chumakov, and R. Rüffer, Phys. Rev. B **58**, 8590 (1998).
[35] R. Röhlsberger, J. Bansmann, V. Senz, K. L. Jonas, A. Bettac, O. Leupold, R. Rüffer, E. Burkel, and K. H. Meiwes-Broer, Phys. Rev. Lett. **86**, 5597 (2001).
[36] U. van Bürck, D. P. Siddons, J. B. Hastings, U. Bergmann, and R. Hollatz, Phys. Rev. B **46**, 6207 (1992).
[37] U. van Bürck, W. Potzel, P. Schindelmann, Yu. V. Shvyd'ko, E. Gerdau, O. Leupold, and H. D. Rüter, Phys. Rev. A **61**, 013803 (2000).
[38] E. F. Kneller and R. Hawig, IEEE Trans. Magn. **27**, 3588 (1991).
[39] E. E. Fullerton, J. S. Jiang, M. Grimsditch, C. H. Sowers, and S. D. Bader, Phys. Rev. B **58**, 12 193 (1998).
[40] R. Skomski and J. M. D. Coey, Phys. Rev. B **48**, 15812 (1993).
[41] K. Mibu, T. Nagahama, T. Shinjo, and T. Ono, Phys. Rev. B **58**, 6442 (1998).
[42] K. V. O'Donovan, J. A. Borchers, C. F. Majkrzak, O. Hellwig, and E. E. Fullerton, Phys. Rev. Lett. **88**, 067201 (2002).
[43] R. Rüffer and A. I. Chumakov, Hyperfine Interact. **97/98**, 589 (1996).
[44] Since the dependence on the azimuthal angle enters as $\cos^2 \phi$ in Eq. (35), fits with $\phi = \pm 45°$, $\phi = 180° \pm 45°$ would fit the data equally well. A determination of the sign is possible using circularly polarized radiation [W. Sturhahn and C. l'Abbe (private communication)].
[45] A. Q. R. Baron, J. Arthur, S. L. Ruby, A. I. Chumakov, G. V. Smirnov, and G. S. Brown, Phys. Rev. B **50**, 10354 (1994).